Chemical states and ferromagnetism in heavily Mn-substituted zinc oxide thin films

Cite as: J. Appl. Phys. **115**, 153902 (2014); https://doi.org/10.1063/1.4871759
Submitted: 13 February 2014 . Accepted: 06 April 2014 . Published Online: 17 April 2014

Q. Shao, P. S. Ku, X. L. Wang, J. A. Zapien, C. W. Leung, F. Borgatti, A. Gambardella, V. Dediu, R. Ciprian, and A. Ruotolo

Chemical states and ferromagnetism in heavily Mn-substituted zinc oxide thin films

Q. Shao,[1] P. S. Ku,[1] X. L. Wang,[1,2] J. A. Zapien,[1,3] C. W. Leung,[4] F. Borgatti,[5] A. Gambardella,[5] V. Dediu,[5] R. Ciprian,[6] and A. Ruotolo[1,a)]
[1]*Department of Physics and Materials Science, City University of Hong Kong, Kowloon, Hong Kong, China*
[2]*State Key Laboratory of Superlattices and Microstructures, Institute of Semiconductors, Chinese Academy of Sciences, Beijing 100083, China*
[3]*Center of Super–Diamond and Advanced Films (COSDAF), City University of Hong Kong, Kowloon, Hong Kong, China*
[4]*Department of Applied Physics and Materials Research Center, Hong Kong Polytechnic University, Hung Hom, Kowloon, Hong Kong, China*
[5]*CNR-ISMN, via Gobetti 101, I-40129 Bologna, Italy*
[6]*Istituto Officina dei Materiali (IOM)-CNR, Laboratorio TASC, Area Science Park, S.S. 14 Km 163.5, I-34149 Trieste, Italy*

(Received 13 February 2014; accepted 6 April 2014; published online 17 April 2014)

A concentration of Manganese as high as 8% was successfully diluted into Zinc Oxide epitaxial films deposited by pulsed laser deposition. The films showed strong ferromagnetism with a large coercivity. Low temperature X-ray absorption spectroscopy measurements indicated that all the Manganese ions substitute for Zinc sites of the wurtzite lattice in the valency of +2. Photoluminescence measurements excluded the presence of Zinc vacancies, as well as Zn interstitials. All the magnetic moments measured were to ascribe to the formation of bound magnetic polarons, with no other contribution due to Manganese-secondary phases or Zinc vacancy-mediated double exchange interaction. © *2014 AIP Publishing LLC*.
[http://dx.doi.org/10.1063/1.4871759]

INTRODUCTION

The growing number of demands for multifunctional devices in the field of information technology supports the development of wide band-gap semiconductors with combined, and possibly correlated, optical and magnetic properties. Direct, wide band-gap semiconductors, which are of fundamental importance for optoelectronics, can be engineered to provide multifunctional magneto-optical materials by doping with magnetic elements.[1] In this perspective, diluted magnetic semiconductors (DMS) could pave the way for a new generation of spin-optoelectronic devices.

Despite the controversies about the origin of the ferromagnetic moment in Manganese-substituted Zinc oxide (Mn:ZnO), this DMS remains a major candidate, particularly after the recent discovery that optical properties in this compound can be tuned by changing the magnetic moment.[2] As compared to other transition-metal diluted semiconductors, Mn:ZnO has several advantages. Since substitutional Mn ions are isovalent to Zn, the concentration of charge carriers is independent on the concentration of spins.[3] As predicted by the bound magnetic polaron (BMP) model, which allows for ferromagnetism in *n*-type ZnO, the magnetic moment of Mn:ZnO can be increased by either increasing the concentration of Mn or the amount of carriers, through introduction of oxygen vacancies.[3,4] This allows ferromagnetism at room temperature in ZnO diluted with small concentration of Mn. A major limitation of this material is its negligible coercivity and remanence at room temperature. This behavior is probably intrinsic in the BMP mechanism, in which isolated BMPs need to be aligned by applying a magnetic field. Remanence and coercivity require a significant overlapping of BMPs that can only be achieved by raising up the concentration of magnetic ions, without introducing lattice defects.

In the present work, we have successfully fabricated films of *n*-type Mn substituted ZnO with concentration of Mn as high as 8% by pulsed laser deposition on ⟨001⟩ sapphire substrates. Detailed description of the structural, chemical, and magnetic properties of these films were achieved by employing several techniques, i.e., X-ray Diffraction (XRD), Photoluminescence (PL), X-ray Photoelectron Spectroscopy (XPS), and X-ray Absorption Spectroscopy (XAS). As a result, we can exclude the presence of Zn vacancies and interstitial Zn in the films, as well as, any significant presence of Mn ions with valence different from +2. The films showed an hysteretic magnetization loop at room temperature, thereby demonstrating the feasibility of increasing the ferromagnetic coupling through a significant concentration of Mn ions and/or oxygen vacancies, without introducing Zn vacancies and other lattice defects.

EXPERIMENTAL DETAILS

A single phase dense $Zn_{1-x}Mn_xO$ ($x = 0.08$) target was prepared via a conventional solid state reaction.[3,5] Briefly, the precursor highly pure ZnO powder (99.999% from Aldrich) and MnO_2 (99.99% from Aldrich) were mixed according to the desired atomic ratio. The powders were grinded by ball milling for 10 hours and then annealed at

a)Author to whom correspondence should be addressed. Electronic mail: aruotolo@cityu.edu.hk

600 °C for 12 h. $Zn_{0.92}Mn_{0.08}O$ films with a thickness of ~100 nm were deposited by pulse laser deposition (PLD) on ⟨001⟩ sapphire substrates. The base pressure in the chamber was better than 10^{-5} millibar. During the PLD deposition, a pulsed KrF excimer laser ($\lambda = 247$ nm) with an energy of 300 mJ operated at a repetition rate of 10 Hz. The substrate was kept at 400 °C. This assures high crystal order and large magnetic moment while preventing the formation of secondary Mn phases.[3] The stoichiometry of both target and films was checked by energy-dispersive X-ray spectroscopy (EDS), which also excluded contamination by unintentional dopants. The crystal structure of the films was investigated by XRD using a Philps X'Pert with Cu Kα radiation source ($\lambda_{Cu} = 0.15406$ nm). Photoluminescence (PL) was used to exclude the presence of Zn interstitial or Zn vacancies. The fourth harmonic of a Nb:yttrium-aluminum-garnet laser ($\lambda = 266$ nm) and 6 ns pulse width was used as the excitation source. Light emission was detected using a 0.5 m spectrometer equipped with a 150 ln/mm grating and an intensified CCD camera (PI-MAX2). The surface of the films was characterized by using a Scanning Tunneling Microscope (STM) operated at room temperature under ultra-high vacuum conditions with a PtIr tip. Scanning Tunneling Spectroscopy (STS) was carried out to verify uniformity of local electrical properties. Electrical characterization was carried out by measuring the four point sheet resistance in magnetic field with a Hall measurement system. XPS measurements were carried out with a 1486.6 eV Al Kα source. Calibration of the energy scale of the spectrometer was obtained by using the adventitious C 1*s* peak at 284.5 eV. X-ray Absorption spectra of the Mn $L_{2,3}$-edges were measured in Total Electron Yield (TEY) mode at the Advanced Photoelectric-effect Experiments (APE) beamline of the Elettra Synchrotron source, in a temperature range of 20–300 K and a base vacuum better than 2×10^{-10} millibar.[6] The incidence angle of the x-ray beam was set at 45° from the surface, with energy resolution of about 0.1 eV. All spectra were normalized by the intensity of the incident beam, which is given by the TEY of a gold mesh. The magnetic properties of the grown films were studied by using a Physical Property Measurement System (PPMS Quantum Design). The hysteresis loops shown in the following are corrected by subtracting the measured linear contribution of the substrate.

RESULTS AND DISCUSSION

Fig. 1 shows the XRD pattern of our films. No detectable traces of secondary Mn_xO_y phase are observed, indicating that all Mn ions are diluted into the host ZnO lattice. The pattern can be indexed by the wurtzite structure of ZnO (JCPDS Card No. 36-1451). Only the diffraction peaks (002) and (004) from the ZnO wurtzite structure can be observed, indicating high texturization of the films along the *c*-axis. By using the sapphire (006) peak as a reference, we could precisely locate the strongest peak (002) of ZnO film at $2\theta = 34.26°$, whereas the same peak for the pure ZnO bulk is expected to be at $2\theta = 34.42°$. A shift of $\Delta\theta = 0.16°$ corresponds to an increase 0.0012 nm of the lattice constant along the *c*-axis, owing to the larger ionic radius of Mn^{2+} (0.066 nm) as compared to that of Zn^{2+} (0.060 nm). The size of the crystal grains was estimated to be ~45 nm, as calculated by using Debye–Scherrer formula $D_{hkl} = 0.9\ \lambda_{Cu}/\beta\ \cos\theta$, with $\beta = 0.826$ full-width half-maximum of the (002) peak.

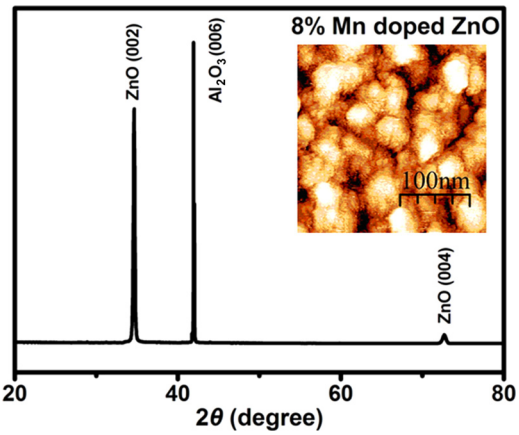

FIG. 1. XRD of an 8% Mn substituted ZnO film grown on sapphire substrate. Inset shows a STM topographic image of the film surface.

The STM topographic scan (Fig. 1, inset) confirmed a polycrystalline morphology, with a grain size that matches well with that calculated by Debye–Scherrer formula. The root-mean-square roughness estimated on a $2 \times 2\ \mu m^2$ scan was 0.65 nm, with a maximum peak-to-peak roughness of 4 nm. Tunnel conductivity maps (not shown here) did not show recognizable spatial patterns, suggesting that local spectroscopic properties are highly uniform and not affected by topographic features. The current-voltage curves showed a metallic-like behavior, suggesting a high concentration of charge carriers induced by oxygen vacancies.

According to the BMP model, magnetism in Mn-substituted ZnO is carrier mediated, whereas Dietl's model predicts room temperature magnetism only in *p*-type ZnO. It is therefore important to determine the type of conduction and the carrier concentration in the films. Fig. 2(a) shows the resistivity and carrier density measured in the temperature range of 10–260 K by using the Hall effect in van der Pauw geometry. The films present *n*-type character with a carrier density of $4.25 \times 10^{17}\ cm^{-3}$ at 260 K. It is important to notice that if Mn is isovalent to Zn in the wurtzite ZnO, no effect of Mn substitution in the conductivity of such films is expected to occur. On the opposite, oxygen vacancies are double donors and, in films grown under the conditions used in this work, they would become the dominant carriers.[3]

A large concentration of native oxygen-vacancy (V_O) donors can mask the presence of deep acceptors due to Zn interstitial (Zn_{in}) or Zn vacancies (V_{Zn}). It is particularly important to exclude the presence of V_{Zn}'s because they can mediate double-exchange interaction between Mn^{2+} ions.[7] For this reason, room temperature PL measurements were carried out in a wide range of wavelength (Fig. 2(b)). It is generally known that luminescence peaks at green-yellow band are easily produced in ZnO film due to deep level transitions between shallow donors (oxygen vacancies) and deep acceptors (Zn vacancies),[8,9] as well as the recombination of shallow donors with residual acceptors (interstitial Zn or impurities).[10] We only detect the near band emission peak of

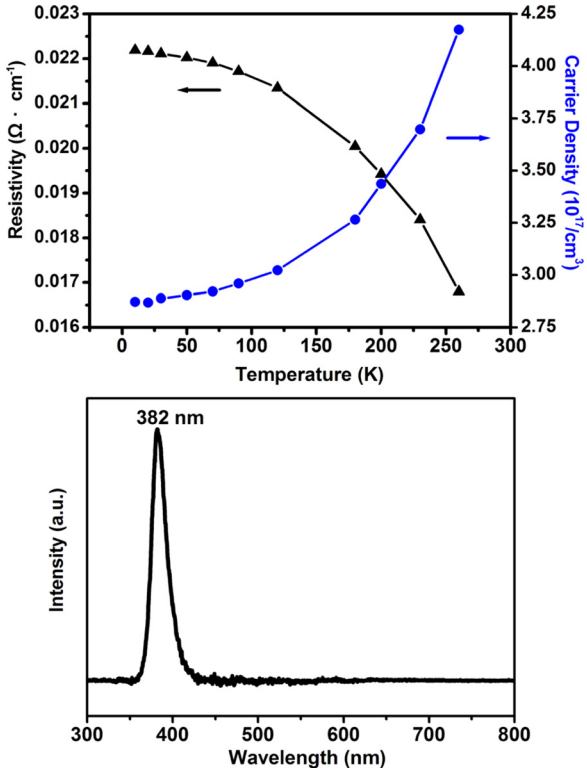

FIG. 2. (a) Temperature dependence of resistivity and carrier density of a typical sample; (b) Room temperature PL spectrum of a typical film.

ZnO, denoting the absence of Zn vacancies and interstitial Zn in the films.

In order to obtain a deeper understanding of the composition and chemical states of the films, XPS and XAS were carried out. Fig. 3(a) shows a typical XPS survey scan of the films. We could detect only the presence of the expected elements, Zn, O and Mn. The positions of the peaks match well with the literature values.[11] The energy distributions of the emitted core-level electrons observed by XPS of Zn in the prepared samples are shown in Fig. 3(b). The double spectral lines of Zn $2p_{3/2}$ and Zn $2p_{1/2}$ are located at 1021.44 eV and 1044.60 eV, respectively, corresponding to the binding energy of Zn^{2+} in ZnO.[12] The O 1s peak, shown in Fig. 3(c), presents many spectral contributions that were successfully disentangled by fitting analysis, resulting in three nearly Gaussian components centered at 530.2 eV (O_a), 531.4 eV (O_b), and 532.6 eV (O_c) and having a standard deviation of 0.42, 0.44, and 0.57, respectively. The strongest O_a peak of the O 1s spectrum is attributed to the Zn-O bonds in ZnO lattice, while the O_b peak at medium binding energy is usually attributed to oxygen vacancies, and the weakest O_c peak concerns surface chemisorbed or dissociated oxygen or OH species, such as adsorbed O_2.[13,14] The ratio of the O_a/O_b integrated intensities is 2.5, therefore a large number of oxygen vacancies have been introduced into the film during growth under the chosen conditions.

Considering that the binding energy of Mn 2p3/2 in Mn metal (Mn^0), Mn^{2+} in MnO, Mn^{3+} in Mn_2O_3, Mn^{3+} in Mn_3O_4, and Mn^{4+} in MnO_2 are located at 638.8 eV, 641.0 eV, 641.4 eV, 641.2 eV, and 642.4 eV, respectively, the peak positions of the Mn 2p spectrum shown in Fig. 3(d) allows us to reliably exclude the presence of Mn in valence 0 and +4 in our sample.[15] The relative low quality of the Mn spectrum, which is mostly influenced by the small photoionization cross section of the Mn 2p core levels, as well as, by the relatively low amount of the ions in the material, hinders us from reliably exclude the presence of Mn in valence +3. More reliable information

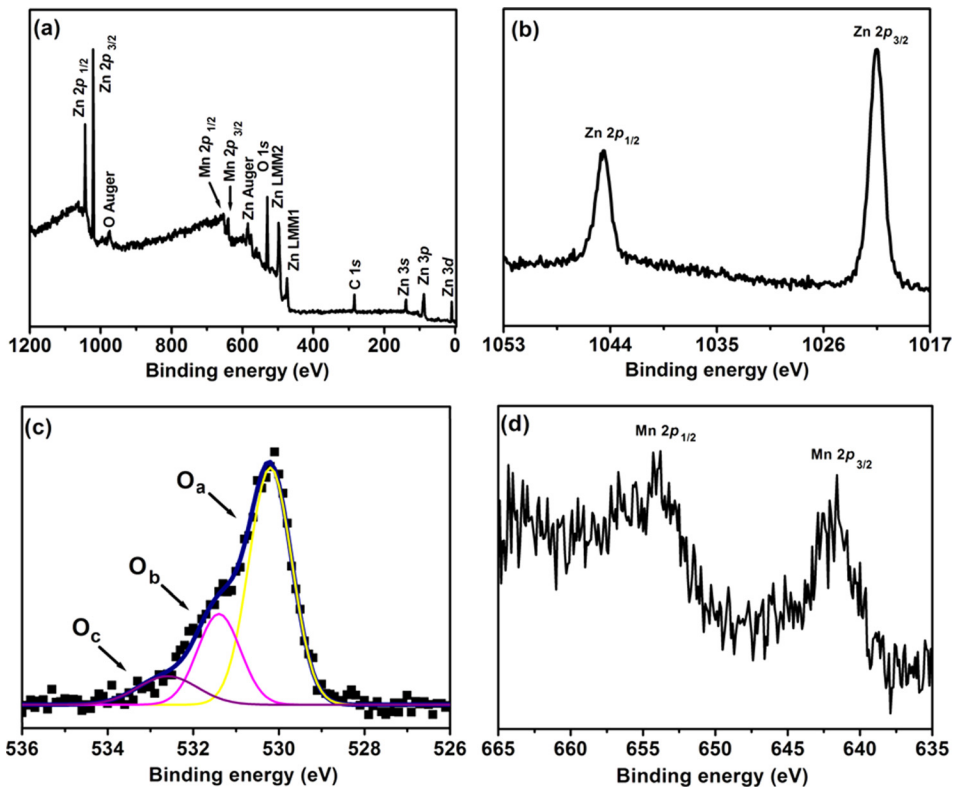

FIG. 3. (a) A typical wide-scan spectrum of a film; (b) XPS spectra of the Zn 2p peaks; (c) XPS spectra of the O 1s peaks; (d) XPS spectra of the Mn 2p peaks.

about the electronic structure and valence state of the Mn ions has been obtanied by soft XAS.

The XAS spectra of the Mn $L_{2,3}$-edges measured at 20 K and 300 K are shown in Fig. 4. The structured lineshape of the spectra is directly correlated to the chemical state, and the local coordination symmetry of the Mn ions dispersed in the ZnO lattice. The spectra are basically identical, hence the chemical state of the Mn in the ZnO is stable across this temperature range. The experimental spectra are compared to atomic multiplet calculations performed in intermediate coupling for different Mn ground-state valence configurations, namely with with $3d^5$ (2+), $3d^4$ (3+), and $3d^3$ (4+) orbital occupancy, using the codes developed by R. D. Cowan *et al.* and modified by Thole.[16] The theoretical Mn $L_{2,3}$ XAS spectra were obtained from the electric-dipole-allowed transitions between the ground-state $3d^n$ and the final-state $2p^53d^{n+1}$ configurations including crystal field effects for local tetrahedral symmetry with $10Dq(T_d) = 0.45$ eV. The Slater and spin-orbit parameters were chosen as in Ref. 17. The calculated spectra include a Lorentzian FWHM of 0.2 (0.4) eV for the L_3 (L_2) edge to account for intrinsic linewidth broadening, and a Gaussian FWHM of 0.1 eV for instrumental broadening. To easily compare the lineshapes, both experimental and theoretical spectra are aligned in energy with respect to the peak with maximum intensity. It looks evident that the shoulder at about 640 eV in the vicinity of the L_3 edge and the double peak structure of the L_2 edge around 650 eV are clear signatures of Mn^{2+} valence state, confirming that substitution at the Zn sites is the leading mechanism for the distribution of the Mn ions within the ZnO host, in close agreement with previous XAS studies for lower Mn concentrations.[18]

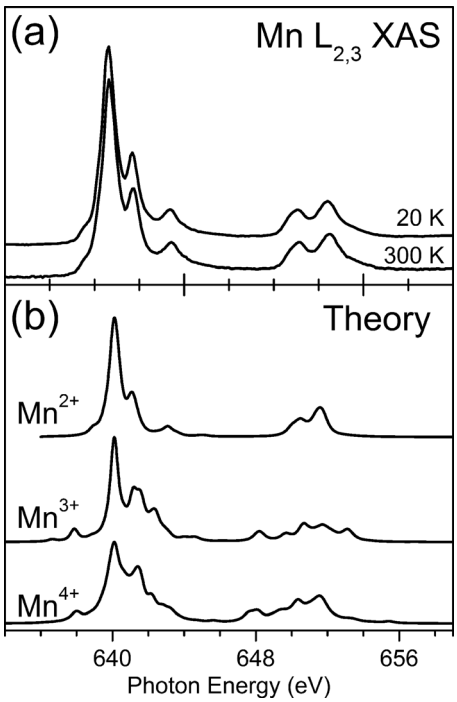

FIG. 4. (a) Mn $L_{2,3}$ XAS measurements at 20 K and 300 K, and (b) multiplet calculations for different valence ground-states in T_d symmetry ($10Dq = 0.45$ eV). Spectra are aligned to the position of the maximum peak intensity.

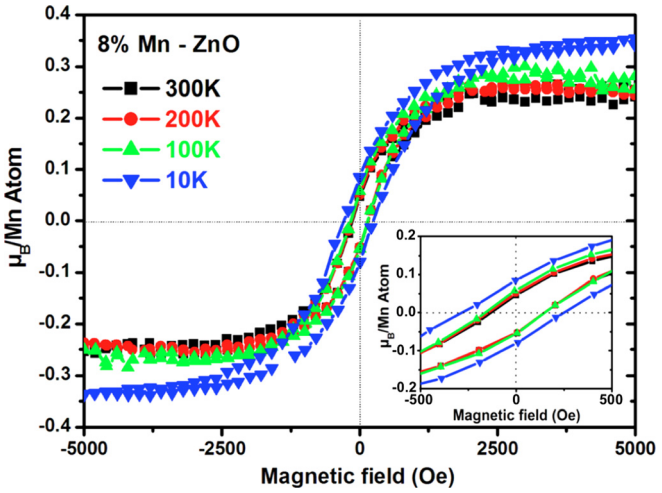

FIG. 5. *M* vs *H* loops measured at different *T*. Inset shows the expanded low-field region of the same loop.

Fig. 5 shows the magnetization loops taken at various temperatures with magnetic field applied in the film plane. The magnetization shows a clear hysteresis even at 300 K with a coercive field of about 130 Oe. The coercive field increases to 254 Oe at 20 K. The saturation magnetic moment per Mn atom at 300 K is 0.23 μ_B/Mn^{2+} and increase up to 0.35 μ_B/Mn^{2+} at 10 K. The values of the magnetic moments that we report here are of particular importance and can be considered as a reliable reference for future studies. Values reported in literature tend to vary significantly, even between samples prepared with the same method. This is because Mn-related secondary phases and V_{Zn}-mediated exchange interaction between Mn^{2+} ions can give a significant contribution at low temperatures. This contribution is not trivial to estimate because the same Mn-secondary phase can show either antiferromagnetic or ferromagnetic behavior depending on the temperature (for a review, see Ref. 19) and on the concentration of V_O's. Moreover, while the presence of V_{Zn} can reliably be excluded by using PL measurements, it is not trivial to estimate the concentration of V_{Zn}'s, in case they are present. We have carried out extensive characterization of our films to reliably exclude any secondary contribution to the magnetic moment at low temperature. The entire moment we measure must be due to overlapping of BMPs.[4] Such overlapping requires the existence of an impurity band and delocalization of the carriers in the impurity band on the magnetic ions. A significant concentration of double donor V_O's provides an impurity band that overlaps (hybridization) with unoccupied *d*-levels of the magnetic dopant, hence favoring a ferromagnetic alignment.

CONCLUSION

We successfully grew high quality 8%-Mn-substituted ZnO films by PLD on single phase (001) sapphire substrates. The films present an hysteretic magnetization loop at room temperature which can be ascribed to formation of BMPs, due to the presence of a significant concentration of oxygen vacancies in the film. Ferromagnetism in this compound is genuine, and the material could find use in magneto-optics.

XRD and EDS results exclude the presence of unintentional magnetic dopants, while photoluminescence measurements exclude the presence of Zn vacancies, and hence of Mn-O-Mn double-exchange interaction. Most of the Mn ions were found with dominant 2+ valence state character, thus excluding precipitation of Mn-secondary phases. The challenge is to increase the ferromagnetic coupling by increasing the concentration of Mn ions, as well as the concentration of oxygen vacancies, without introducing Zn vacancies and other lattice defects.

ACKNOWLEDGMENTS

The work described in this paper was supported by the Research Grants Council of the Hong Kong Special Administrative Region, China [Grant Nos. CityU102711 and CityU 104512] and by the National Science Foundation of China (NSFC), [Grant No. 11274261]. Financial support from the European Union Council under the 7th Framework Program (FP7) Grant No. 246102 IFOX is also acknowledged.

[1]S. J. Pearton, C. R. Abernathy, M. E. Overberg, G. T. Thaler, and D. P. Norton, J. Appl. Phys. **93**, 1 (2003).
[2]X. L. Wang, C. Y. Luan, Q. Shao, A. Pruna, C. W. Leung, R. Lortz, J. A. Zapien, and A. Ruotolo, Appl. Phys. Lett. **102**, 102112 (2013).
[3]X. L. Wang, K. H. Lai, and A. Ruotolo, J. Alloys Compd. **542**, 147 (2012).
[4]J. M. D. Coey, M. Venkatesan, and C. B. Fitzgerald, Nature Mater. **4**, 173 (2005).
[5]P. Sharma, A. Gupta, K. V. Rao, F. J. Owens, R. Sharma, R. Ahuja, J. M. O. Guillen, B. Johansson, and G. A. Gehring, Nature Mater. **2**, 673 (2003).
[6]G. Panaccione, I. Vobornik, J. Fujii, D. Krizmancic, E. Annese, L. Giovanelli, F. Maccherozzi, F. Salvador, A. De Luisa, D. Benedetti, A. Gruden, P. Bertoch, F. Polack, D. Cocco, G. Sostero, B. Diviacco, M. Hochstrasser, U. Maier, D. Pescia, C. H. Back, T. Greber, J. Osterwalder, M. Galaktionov, M. Sancrotti, and G. Rossi, Rev. Sci. Instrum. **80**, 043105 (2009).
[7]J. B. Yi, C. C. Lim, G. Z. Xing, H. M. Fan, L. H. Van, S. L. Huang, K. S. Yang, X. L. Huang, X. B. Qin, B. Y. Wang, T. Wu, L. Wang, H. T. Zhang, X. Y. Gao, T. Liu, A. T. S. Wee, Y. P. Feng, and J. Ding, Phys. Rev. Lett. **104**, 137201 (2010).
[8]H.-J. Egelhaaf and D. Oelkrug, J. Cryst. Growth **161**, 190 (1996).
[9]B. J. Jin, S. Im, and S. Lee, Thin Solid Films **366**, 107 (2000).
[10]J. Gutowski, N. Presser, and I. Broser, Phys. Rev. B **38**, 9746 (1988).
[11]C. D. Wagner, W. M. Riggs, L. E. Davis, J. F. Moulder, and G. E. Muilenberg, *Handbook of XPS* (Perkin Elmer Corporation, Eden Prairie, Minn, USA, 1979).
[12]J. F. Moulder, W. F. Stickle, P. E. Sobol, and K. D. Bomben, *Handbook of X-Ray Photoelectron Spectroscopy*, edited by J. Chastain and R. C. Kings, Jr. (Physical Electronics, Eden Prairie, MN, 1995).
[13]M. Chen, X. Wang, Y. H. Yu, Z. L. Pei, X. D. Bai, C. Sun, R. F. Huang, and L. S. Wen, Appl. Surf. Sci. **158**, 134 (2000).
[14]S. Major, S. Kumar, M. Bhatnagar, and K. L. Chopra, Appl. Phys. Lett. **49**, 394 (1986).
[15]R. J. Iwanowski, M. H. Heinonen, and E. Janik, Chem. Phys. Lett. **387**, 110 (2004).
[16]F. de Groot and A. Kotani, *Core Level Spectroscopy of Solids* (Taylor & Francis CRC press, 2008).
[17]G. van der Laan and I. W. Kirkman, J. Phys.: Condens. Matter **4**, 4189 (1992).
[18]J. Okabayashi, K. Ono, M. Mizuguchi, M. Oshima, S. S. Gupta, D. D. Sarma, T. Mizokawa, A. Fujimori, M. Yuri, C. T. Chen, T. Fukumura, M. Kawasaki, and H. Koinuma, J. Appl. Phys. **95**, 3573 (2004).
[19]T.-L. Phan and S. C. Yu, J. Phys. Chem. C **117**, 6443 (2013).